Turkish J. Eng. Env. Sci.
32 (2008) , 85 – 100.

A Mathematical Framework for Simulation of Thermal Processing of Materials: Application to Steel Quenching

Caner ŞİMŞİR
Stiftung Institut für Werkstofftechnik Badgasteiner Str. 3
28359 Bremen-GERMANY
e-mail: simsir@iwt-bremen.de
Cemil Hakan GÜR
Middle East Technical University, Department of Metallurgical and Materials Engineering
Ankara-TURKEY

Received 03.09.2007

Abstract

During thermal processing, parts are usually subjected to continuous heating and cooling cycles during which microstructural and mechanical evolutions occur simultaneously at different length and time scales. Modeling of these processes necessitates dealing with inherent complexities such as large material property variations, complex couplings and domains, combined heat and mass transfer mechanisms, phase transformations, and complex boundary conditions. In this study, a finite element method based mathematical framework capable of predicting temperature history, evolution of phases and internal stresses during thermal processing of materials was developed. The model was integrated into the commercial FE software MSC.Marc® by user subroutines. The accuracy of the model was verified by simulating the quenching of hollow steel cylinders. Simulation results were compared with SEM observations and XRD residual stress measurements. According to the results, the model can effectively predict the trends in the distribution of microstructure and residual stresses with remarkable accuracy.

Key words: Thermal Processing, Modeling, Simulation, Quenching, Steel

Introduction

Thermal processing of materials refers to manufacturing and material fabrication techniques that are strongly dependent on the thermal transport mechanisms. With the substantial growth in new and advanced materials like composites, ceramics, different types of polymers and glass, coatings, specialized alloys, and semiconductor materials, thermal processing has become particularly important since the properties and characteristics of the product, as well as the operation of the system, are largely determined by heat transfer mechanisms (Jaluria, 2003).

A few important materials processing techniques in which heat transfer plays a very important role are listed in Table 1. The list contains both traditional processes and new or emerging methods. In the former category, welding, metal forming, polymer extrusion, casting, heat treatment, and drying can be included. The rest may be included in the latter category.

The dependence of the properties of the final product on the physics of the process must be clearly understood so that analysis or experimentation can be used to design processes to achieve optimum quality at desired production rates. Modeling is one of the most crucial elements in the design and optimization of thermal materials processing systems.

Mathematical and numerical modeling of thermal processing of materials is a challenging task. A model must deal with at least one or several of the following difficulties:

Table 1. Examples of thermal processing of materials.

Process Category	Examples
Solidification	Casting, continuous casting, crystal growing
Heat Treatment	Annealing, hardening, tempering, surface treatments, curing, baking
Forming	Hot rolling, wire drawing, metal forming, extrusion, forging, press forming, injection molding, thermoforming, glass blowing
Bonding	Soldering, welding, chemical-diffusion bonding
Coating	Thermal spray coating, polymer coating
Powder Processing	Powder metallurgy, ceramic processing, sintering, sputtering
Other	Composite materials processing, microgravity materials processing, rapid prototyping

- The model may require dealing with highly nonlinear material properties since material properties usually have a pronounced variation with temperature, stress, and concentration.
- The model may require including couplings between different physical events such as heat/mass transfer, mechanical interactions, phase transformations, and chemical reactions.
- The model may require handling of multiscale couplings due to mechanisms operating at different length and time scales.
- The model may necessitate handling of complex geometries and domains since engineering systems for thermal processing usually involve complex geometries with multiple domains.
- The model may require dealing with complex boundary conditions such as highly nonlinear and moving boundary conditions.
- The model may necessitate handling of different energy sources ranging from conventional heating to laser, induction, gas, fluid jet heating/cooling.

In this study, a flexible mathematical framework for simulation of thermal processing of materials, capable of dealing with most of the above difficulties, is developed and integrated into commercial finite element analysis software MSC.Marc® by user subroutines. The framework has a modular structure and allows coupling of different simulation and numerical solution techniques with FEM. As a case study, the model is verified by simulating the quenching of hollow C60 steel cylinders from 830 °C into 20 °C water. Simulation results were compared with SEM inspection and residual stress measurements.

Mathematical Framework

Thermal processing of materials is a complex multiscale and multiphysics problem. During the thermal processing of materials, parts are usually subjected to continuous heating and cooling cycles during which microstructural and mechanical evolutions occur simultaneously at different length scales. Each physical field is described by governing equations and an appropriate set of initial and boundary conditions. Most of those equations have a nonlinear nature. In addition, physical fields interact with each other either by sharing of state variables or by coupling interactions. Figure 1 is a brief representation of physical fields and couplings during the thermal processing of materials.

Analytical solution of coupled nonlinear equations is usually not possible. The rigorous treatment of the problem requires a coupled total thermo-mechano-microstructural theory. However, a commonly accepted incorporation of the kinetics and irreversible thermodynamics of the phase transformations in such a coupled theory has not been done so far. As a remedy, a "staggered numerical solution" of the problem is suggested in this study.

The currently developed framework consists of a modular system, in which each module deals with a certain physical field and related couplings. The solution may involve the application of numerical methods such as the finite difference method (FDM), finite volume method (FVM), and finite element method (FEM). In this study, FEM is used for numerical solution of most of the physical fields such as thermal and mechanical fields because of its wide spectrum of applicability and ease of use. FDM is used for the solution of anisothermal kinetics of phase transformations.

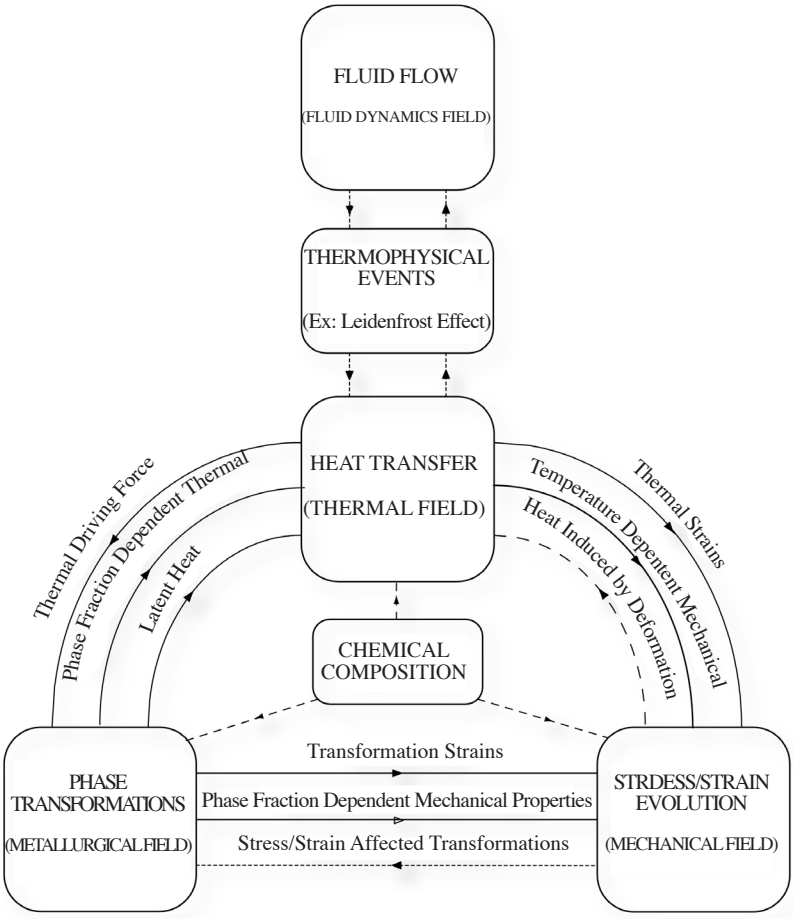

Figure 1. A general representation of physical fields and interactions during thermal processing of materials.

The simplest case of thermal processing of materials involves coupled calculation of heat transfer and microstructural evolution. This type of coupling may be sufficient if the phase transformations are not highly affected by stress/strain and the calculation of mechanical interactions (stresses/strains) is not important. However, in most industrial cases, this assumption is not valid at all. A much more realistic case involves the calculation of heat transfer, and microstructural and mechanical evolution. This case covers many thermal treatments applied to engineering materials. Formulation of the mechanical field may involve elastic stress/strain analysis, e.g., thermal processing of ceramics, an elastoplastic analysis, e.g., heat treatment of metals and alloys, or viscoelastoplastic analysis, e.g., thermal processing of polymers, processes involving slow cooling rates. Due to its flexible and modular design, all of these couplings and variations may be incorporated into the current framework with minor revisions.

Another advantage of the current framework lies in its ability to deal with multiscale treatment of certain phenomena such as phase transformations and transformation plasticity since the phase transformation module runs on an integration point basis. Lower scale simulations (mesoscopic or atomistic) can be performed using a representative volume elements (RVE) and proper scale shifting methods. In addition, the current framework allows the coupling of the heat transfer field with other physical fields controlling heat transfer. For example, heat transfer from the surface is controlled by fluid flow around the component in many cases. Convective cooling rates are highly dependent on the fluid flow velocity, the viscosity, and the heat capacity of the process medium. Computational fluid dynamics (CFD) calculations may be coupled to determine actual surface heat flux. A weak coupling of fluid flow field with thermo-mechano-microstructural analysis may be created by importing the mass flow

rate of the fluid calculated in a CFD program such as FLUENT® and CFX® as a function of position and time and applying this information as the thermal boundary condition. Another example of a physical event controlling the heat transfer may be illustrated in induction heating of ferrous alloys, during which magneto-electrical heating drives the heat transfer. This kind of simulation may allow engineers to optimize the system to optimize the distortion, residual stress, and microstructure distribution.

Chemical composition (diffusion) field is also another important physical field that should be taken into account for simulation of thermal processes during which the chemical composition is not macroscopically homogeneous. This field involves the solution to Fick's diffusion equation. This field is not currently incorporated into the developed framework. Its incorporation may allow the simulation of thermo-chemical surface treatments such as carburizing and nitriding of steel components.

Physical fields and coupling interactions

Heat transfer is the major driving event triggering the other events. Heat transfer from the surface is highly dependent on the transfer mechanisms (conduction, convection, and radiation), fluid flow, and thermo-physical and thermo-chemical processes occurring at the interface. Other important physical events of the thermal processing of materials are phase transformations and the generation of an internal stress field due to thermal gradients and phase transformations.

Thermal stresses are generated in the thermally processed material due to large temperature gradients and the variation in mechanical properties with temperature. Varying heating/cooling rates at different points lead to varying thermal expansions/contractions, which must be balanced by an internal stress state. Those stresses may cause nonuniform plastic flow when their magnitude at any point exceeds local yield strength. On the other hand, plastic deformation causes heat generation due to internal friction. However, heat induced by deformation is usually negligible since plastic deformations are relatively small (2%-3%) during thermal treatments.

Variation in temperature at any point in thermally processed material is the major driving force for phase transformations. Upon treatment, the thermodynamic stability of the parent phase is altered, which results in decomposition of the parent phase into transformation products. The transformation rate basically depends on the temperature and the cooling/heating rate. On the other hand, there exists a heat interaction with the surroundings during phase transformations. Phase transformations that occur during quenching are exothermic and they alter the thermal field by releasing latent heat of transformation. It has been shown that neglecting this effect has a strong side effect on the accuracy of the determination of the temperature field (Denis et al., 1992).

Typically, a material undergoing a heat treatment is subjected to a fluctuating triaxial stress state and small plastic strains (up to 2%-3%) due to thermal stresses and phase transformations. These strains may be due to density change, elastic coherency, or transformation induced plasticity (TRIP). TRIP is the significantly increased plasticity during a phase change. Even for an externally applied load for which the corresponding equivalent stress is small compared to the normal yield stress of the material, plastic deformation occurs. This phenomenon is explained by the existence of an irreversible strain resulting from phase transformation under stress. TRIP is currently explained by the competition of 2 mechanisms depending on thermo-mechanical loading conditions (Cherkaoui, 2002):

- *Plastic Accommodation (Greenwood-Johnson) Mechanism:* During phase transformations under a stress field, the interaction of the load stress and the geometrically necessary stress to accommodate the transformation eigenstrain results in an irreversible strain. This pioneering explanation of TRIP was given by Greenwood and Johnson (1965). This mechanism is operational for both displacive (martensitic) and reconstructive (diffusional) phase transformations.

- *Variant Selection (Magee) Mechanism:* Martensitic transformation from FCC to BCC (and BCT) crystal structure occurs with 24 possible variants, each characterized by a distinct lattice orientation relationship. At the mesoscopic scale, each variant is defined by a transformation strain involving a dilatational (δ) component perpendicular to the habit plane and a shear component (γ) on the habit plane. In general, only the preferred variants are nucleated upon thermo-mechanical loading depending on the stress state. The earliest observation of this mechanism based on variant

selection was in the works by Patel and Cohen (1953). Later, this mechanism was called the "Magee" mechanism due to his famous study on the importance of formation of preferred variants in iron based alloys (Magee, 1966).

Phase transformations that occur under stress and with prior or concomitant plasticity can be considered examples of 'materials systems under driving forces' in which both the driving forces for transition and the kinetics of the process can be altered by mechanical interactions. The interaction of mechanical driving forces and phase transformations depends both on the material and loading conditions. For example, the thermodynamics of phase transformations, i.e. transformation temperatures, and chemical composition of parent and product phases, is modified by the change in free energies of parent and product phases. Similarly, kinetics of transformation, i.e. transformation rates, path of transformation, may also be altered because of the change in the mobility of atoms due to elastic and plastic strains. Elastic strains affect the kinetics of transformation by changing the mobility of atoms by changing the free volume. Plasticity alters the transport processes by changing the point defect concentration, providing shortcuts for diffusion via dislocation cores or by providing a nondiffusive transport mechanism where the atoms are convected by moving dislocations either geometrically or via the drag effect due to dislocation/solute interaction (Embury et al., 2003).

First observations and modeling studies in the field are focused on the effect of stress and plastic deformation on martensitic transformations. It has been observed that a uniaxial stress leads to an increase in M_s, whereas hydrostatic pressure and plastic deformation results in a decrease. However, a plastic strain of 1%-3%, which is common in thermal processing of metals and alloys, only causes a change of a few degrees but a stress close to the yield strength of the parent phase leads to a change of 30-50 °C. Thus, for the purpose of simulation of thermal processing, during which large stresses and small plastic strains are characteristic, the effect of plastic strain on M_s may be neglected.

Formulation of thermal field

Accurate prediction of thermal history is vital for simulation purposes and accurate results can only be obtained by deep understanding of the heat transfer phenomenon. The accuracy of the thermal history prediction influences directly the accuracy of phase transformation kinetics, and thermal and phase transformation stress calculations. A poor heat transfer model or inaccurate heat transfer data will eventually result in considerable errors in the predicted microstructure and stresses even though the phase transformation and mechanical modules are functioning perfectly.

The transient heat transfer within the material during thermal processing can be described mathematically by an appropriate form of Fourier's heat conduction equation. Considering that the thermal field is altered by latent heat of phase transformations, the equation can be expressed in its most general form as

$$\rho c \frac{\partial T}{\partial t} = div(\lambda \nabla T) + Q \tag{2.1}$$

where ρ, c_p, and λ are the density, specific heat, and thermal conductivity of the phase mixture given as a function of temperature, respectively. Q is the internal heat source/sink term due to latent heat released per unit mass, which is a function of transformation rate and temperature as

$$\dot{Q} = L_k \dot{\xi}_k \tag{2.2}$$

where L is the latent heat of transformation.

Thermal properties of the phase mixture may be approximated by a linear rule of mixture

$$P(T, \xi_k) = \sum_{1}^{N} P_k \xi_k \tag{2.3}$$

where P represents an average thermal property of the mixture, and P_k is a thermal property of the k^{th} constituent of the phase mixture. ξ_k is the volume fraction of the k^{th} constituent.

The energy change (i.e. the temperature drop) due to adiabatic expansion and the energy due to plastic flow are also neglected. Simple estimates show that their contribution to heat generation rate terms is less than 1% for nearly incompressible solids (Sjostrom, 1984).

Finally, initial and boundary conditions must be set to complete the definition of the thermal problem. A surface temperature dependent convective heat transfer boundary condition can be defined as

$$\Phi(T_s, T_\infty) = h(T_s)(T_s - T_\infty) \tag{2.4}$$

where Φ is the heat flux from the surface, which is a function of surface and the quenchant temperature. $h(T_s)$ is the surface temperature dependent

heat transfer coefficient. Use of a surface temperature dependent heat transfer coefficient permits us to incorporate the effect of different cooling rates at different stages of heat treatment. Similarly, a radiation boundary condition can be defined as

$$\Phi(T_s, T_\infty) = k_B \zeta (T_s^4 - T_\infty^4) \tag{2.5}$$

where ζ is the emissivity of the surface and k_B is the Stephan-Boltzmann constant.

An insulated boundary can be specified by setting the heat flux to 0 by

$$\Phi = -\lambda \frac{\partial T}{\partial n} = 0 \tag{2.6}$$

where $\partial T/\partial n$ is the directional derivative of the temperature in the outer normal (n) direction.

Formulation of microstructural field

Several mathematical models have been proposed for mathematical description of the isothermal transformation kinetics of solid state transformations, most of which are based on the same principles with minor modifications. In these models, the transformed fraction is expressed by

$$\xi_k = \begin{cases} 1 - exp\left(-b_k t^{n_k}\right) & ;\ r = 1 \text{ (Avrami)} \\ 1 - \left(1 + b_k t^{n_k}\right)^{-1} & ;\ r = 2 \text{ (Austin-Rickett)} \\ 1 - \left(1 + (r_k - 1)\, b_k t\right)^{\left(\frac{r_k - 1}{n_k}\right)} & ;\ r \neq 1 \end{cases} \tag{2.7}$$

where b, n, and r are temperature dependent time coefficient, time exponent, and saturation parameter, respectively. n depends on the ratio of nucleation and growth rates, whereas b depends on the absolute values of nucleation and growth rate. r depends on the growth mode and the temperature, and different choices result in different kinetic equations. For example, the equation obtained is the Avrami equation when r = 1 and the Austin-Rickett equation when r = 2 (Avrami, 1939).

The Johnson-Mehl-Avrami-Kolmogorov (JMAK) equation may be corrected to account for phase transformations that start from a phase mixture and do not saturate to 100% as

$$\xi_k = \xi_k^o + \left(\xi_k^{eq} - \xi_k^o\right)\left(1 - \exp\left(b_k t^{n_k}\right)\right) \tag{2.8}$$

where ξ^o and ξ^{eq} are the initial and the equilibrium concentrations.

Equation (2.8) can be further improved to deal with anisothermal kinetics of phase transformations by Scheil's additivity principle, which was later extended to solid state phase transformation by Cahn (1956) and generalized by Christian (1975). According to Scheil's additivity rule, if $\tau(\xi_k,T)$ is the isothermal time required to reach a certain transformed amount ξ_k, the same transformation amount will be reached under anisothermal conditions when the following Scheil's sum (S) equals unity (Scheil, 1935):

$$S = \int_0^t \frac{dt}{\tau(\xi_k, T)} = 1 \tag{2.9}$$

This rule can be exploited in the calculation of both the incubation times and the anisothermal kinetics of transformations. The calculation of incubation time, as summarized in Figure 2, is straightforward; replacing $\tau(\xi_k, T_i)$with isothermal incubation time $(\tau_s(T_i))$ results in

$$S = \sum_{i=1}^{n} \frac{\Delta t_i}{\tau_s(T_i)} \approx 1 \tag{2.10}$$

The incubation is considered complete when S equals unity.

After the completion of incubation, growth kinetics is calculated, which is illustrated in Figure 7. Considering the Avrami kinetic equation, a fictitious time τ, which is dependent on the fraction transformed up to the end of the previous time step, is calculated by

$$\tau = \left(-\frac{\ln\left(1 - \xi_k(t)\right)}{b_k}\right)^{\frac{1}{n_k}} \tag{2.11}$$

Next, the fictitious time is incremented by time step size (Δt) in order to calculate a new fictitious transformed fraction. Using the fictitious transformed fraction, actual transformed amount is calculated by

$$\xi_k^{t+\Delta t} = \xi_k^{\max}\left(\xi_\gamma^t - \xi_k^t\right)\left(1 - \exp\left(b_k\left(\tau + \Delta t\right)^{n_k}\right)\right) \tag{2.12}$$

where $\xi_k^{\max}$is the maximum fraction of the product phase. In the case of transformations that do not saturate to 100% completion $\xi_p^{\max}$can be calculated using the lever rule in the equilibrium phase diagram.

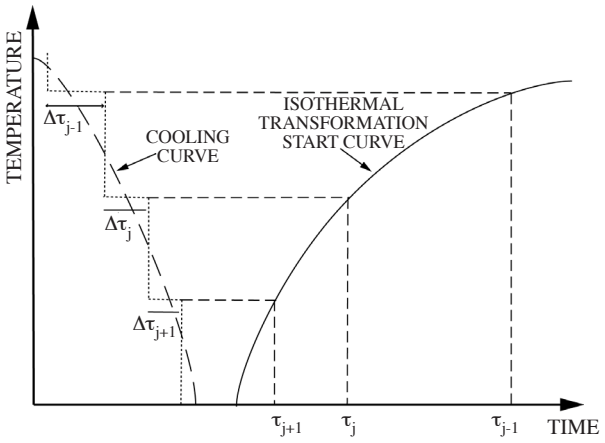

Figure 2. Schematic representation of calculation of anisothermal incubation time from TTT diagram using Scheil's additivity principle.

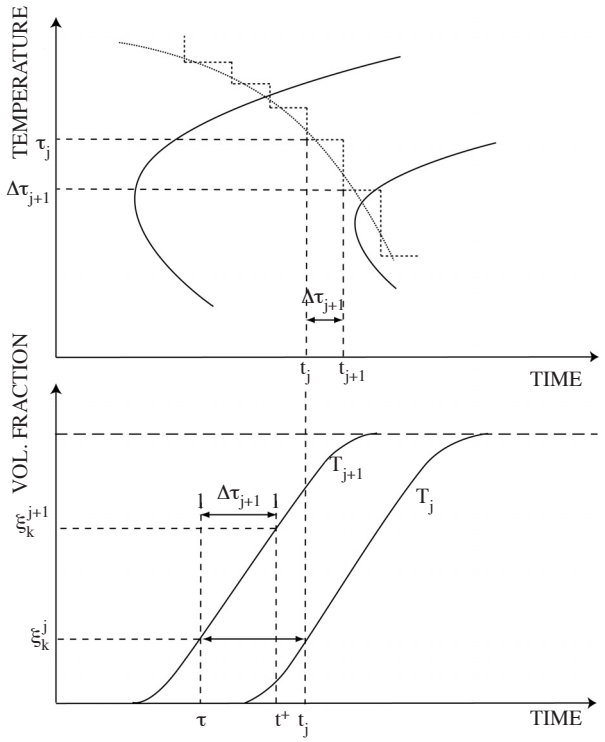

Figure 3. Schematic representation of calculation of anisothermal growth kinetics from isothermal kinetics by Scheil's additivity principle.

This expression may be further improved to take into account the effect of stress on diffusional phase transformations. For example, Hsu (2005) proposed a modified JMAK equation in which both the coefficient (b) and the exponent (n) of kinetic equation are functions of effective stress as

$$\xi_p = \xi_\gamma . \left(1 - \exp\left(-b(\bar{\sigma}) t^{n(\sigma)}\right)\right) \tag{2.13}$$

$$b(\bar{\sigma}) = b(0)(1 + A\bar{\sigma}^B) \tag{2.14}$$

$$n(\bar{\sigma}) = n(0) \tag{2.15}$$

where parameters A and B can only be determined by regression of experimental data and are dependent on the material and phase transformation type. b(0) and n(0) can be calculated from TTT data.

Modeling the martensitic (displacive) transformations Martensite is generally considered to form by a time independent transformation below M_s temperature. Therefore, its kinetics is essentially not influenced by the cooling rate and cannot be described by Avrami type of kinetic equations. The amount of martensite formed is often calculated as a function of temperature using the law established by Koistinen and Marburger (1959),

$$\xi_m = \xi_\gamma \left(1 - \exp\left(-\Omega \left(M_s - T\right)\right)\right) \tag{2.16}$$

where Ω is a material constant, whose value is 0.011 for many steels regardless of chemical composition.

It should also be noted that M_s temperature is also dependent on the stress state, prior to plastic deformation. Various models have been developed for quantitative description of the effect of stress on martensitic transformations (Inoue and Wang, 1982; Loshkarev, 1986; Denis et al., 1987). Most of them are based on modification critical temperatures and the Koistinen-Marburger law. Inoue (Inoue and Wang, 1985) proposed a model in which the change in M_s (ΔM_s) is a function of mean stress (σ_m) and the second invariant of deviatoric stress tensor (J_2). According to his model, the change in M_s is described as

$$\Delta M_s = A\sigma_m + BJ_2^{1/2} \tag{2.17}$$

where A and B material are dependent constants that can be determined experimentally.

Formulation of mechanical field

Material models that have been proposed for simulation of thermal processing of materials can be classified into elastoplastic, elasto-viscoplastic, and unified plasticity constitutive models. Almost all of the formulation of constitutive equations is based on the additive decomposition of strain tensor. Rate independent elastoplastic models are the most frequently

used in the simulation of thermal treatments involving relatively high cooling/heating rates. In the literature, there exist several viscoplastic models for simulation of heat treatments (Rammerstorfer et al., 1983; Colonna et al., 1992). However, those models are proposed especially for heat treatments involving slow cooling rates or materials that have pronounced viscoplastic behavior at the treatment temperature range (such as polymers and glass). To describe the elastic-plastic mechanical behavior of the material during a thermal process involving phase transformations, a yield functional (Ψ) using temperature, Cauchy stress (σ_{ij}), volume fraction of phases (ξ_k), and plastic history of the phases (κ_k) as state variables is defined.

$$\Psi = \Psi(T, \sigma_{ij}, \xi_k, \kappa_k) \tag{2.18}$$

To determine the transition from elastic to plastic regime, a von Mises type effective stress ($\bar{\sigma}$) is defined as

$$\bar{\sigma} = \sqrt{\frac{2}{3}\left(S_{ij} - \alpha_{ij}\right)\left(S_{ij} - \alpha_{ij}\right)} \tag{2.19}$$

where S_{ij} and α_{ij} are stress deviator and kinematic hardening (backstress) tensor, respectively.

Then, the von Mises associated flow rule is used by setting the plastic potential functional equal to yield functional (Ψ).

The hardening behavior of a material has isotropic and kinematic components. In combined hardening, both effects are observed. Linear isotropic and kinematic hardening rules can be expressed respectively by

$$\sigma_f = \sigma_0 + H.\bar{\varepsilon}^p \tag{2.20}$$

$$\alpha_{ij} = C\varepsilon^p_{ij} \tag{2.21}$$

where σ_o, H, and C are material parameters depending on the temperature and the fraction of phases.

In the literature, purely isotropic hardening rules are commonly used for simulation of heat treatments. However, the presence of kinematic hardening may have a considerable impact on simulation results due to the loading, unloading, and reverse loading cycle, which is common during thermal processing. There exist several studies reporting that the kinematic hardening rule produces better results in the case of surface treatments such as induction and laser hardening or quenching after thermo-chemical treatments such as carburizing and nitriding during which phase transformations occur only in a part of the component while a large proportion of the component remains unaffected (Rammerstorfer et al., 1981; Sjöström, 1982; Zandona et al., 1993; Denis et al., 1994).

In this study, a special linear isotropic hardening rule considering the effect of phase transformations is suggested since the plastic deformation accumulated in the parent phase will be lost totally or partially during phase transformations. Thus, it is not convenient to use effective plastic strain ($\bar{\varepsilon}^p$) as a strain hardening parameter. Thus, a new strain hardening parameter (κ_k) that tracks the history of the plastic deformation for each phase is defined as follows

$$\kappa_k(\tau + \Delta\tau) = \int_{\tau=0}^{\tau} \left(\dot{\bar{\varepsilon}}^p - \frac{\dot{\xi}_k}{\xi_k}\kappa_k(\tau)\right).d\tau \tag{2.22}$$

where $\kappa_k$is the related strain hardening parameter for the k^{th} constituent and $\dot{\bar{\varepsilon}}^p$is the equivalent strain rate. It should be noted that κ_a is equal to$\bar{\varepsilon}^p$since the parent phase exists from the beginning until the end of transformations. For the other phases, the value of $\kappa_k$is calculated using Eq. (2.22). Then a new variable flow stress for the phase mixture is defined using κ as follows:

$$\sigma_f = \sum_{k=1}^{N} \xi_k.(\sigma_0)_k + \sum_{k=1}^{N} \xi_k.H_k.\kappa_k = \sigma_0 + \sum_{k=1}^{N} \xi_k.H_k.\kappa_k \tag{2.23}$$

After the definition of yield functional, flow rule, and hardening rule, a constitutive law is set in the form of strain rates by summing up the strains caused by different physical sources,

$$\dot{\varepsilon}_{ij} = \dot{\varepsilon}^e_{ij} + \dot{\varepsilon}^p_{ij} + \dot{\varepsilon}^{th}_{ij} + \dot{\varepsilon}^{pt}_{ij} + \dot{\varepsilon}^{tp}_{ij} \tag{2.24}$$

where$\dot{\varepsilon}_{ij}$, $\dot{\varepsilon}^e_{ij}$, $\dot{\varepsilon}^p_{ij}$, $\dot{\varepsilon}^{th}_{ij}$, $\dot{\varepsilon}^{pt}_{ij}$, $\dot{\varepsilon}^{tp}_{ij}$are total, elastic, plastic, thermal, volumetric phase transformation, and transformation plasticity strain rate tensors, which are defined as

$$\dot{\varepsilon}^e_{ij} = \frac{1+\nu}{E}\sigma_{ij} - \frac{\nu}{E}\delta_{ij}\sigma_m \tag{2.25}$$

$$\dot{\varepsilon}^p_{ij} = d\lambda.\frac{\partial\Psi}{\partial\sigma_{ij}} \tag{2.26}$$

$$\dot{\varepsilon}^{th}_{ij} = \alpha.\delta_{ij}.\dot{T} \tag{2.27}$$

$$\dot{\varepsilon}^{pt}_{ij} = \frac{1}{3}\Delta_k\delta_{ij}\dot{\xi}_k \tag{2.28}$$

$$\dot{\varepsilon}^{tp}_{ij} = \frac{3}{2}K_k(1-\xi_k)\dot{\xi}_k S_{ij} \tag{2.29}$$

where υ, E, dλ, α, Δ, K, and S_{ij} are Poisson's ratio, elastic modulus, plastic multiplier, thermal expansion coefficient, structural dilatation due to phase transformation, TRIP constant, and deviatoric part of the Cauchy stress tensor, respectively.

Implementation and Solution Procedure

Simulation of the thermal processing of materials using Msc.Marc involves modification of a coupled thermo-mechanical analysis by incorporation of microstructural evolution effects. Figure 4 illustrates the basic algorithm for incorporation of phase transformation effects and couplings into Msc.Marc.

At the beginning of the analysis, all the material and process data such as thermo-mechanical material properties of each phase and isothermal phase transformation kinetic data are stored in a common block via USDATA subroutine. The temperature distribution in the component is calculated by Msc.Marc at each time step. During the thermal analysis ANKOND and USPCHT subroutines are invoked to incorporate the effect of variation of thermal properties and latent heat due to phase transformations. After the thermal pass, microstructural evolution is calculated in UBGITR subroutine between the thermal and mechanical calculations. In this subroutine, the fraction of each phase is determined using isothermal kinetic data and Scheil's additivity principle. The fraction of each phase is stored in the common blocks and post file using PLOTV subroutine. Thus, transformation strains and latent heat can be calculated and incorporated in the model by the use of constitutive subroutines. Finally, the control is given back to Msc.Marc for mechanical calculations. During the mechanical pass ANEXP, HOOKLW, and WKSLP subroutines are invoked to create thermo-metallo-mechanic couplings. This procedure is repeated at each time step.

Thermal analysis procedure The FEM formulation of the governing equation for a nonlinear transient heat transfer problem with internal heat source is written in the form

$$[H]\left\{\dot{T}\right\} + [C]\{T\} = \{Q\} \tag{3.1}$$

where [H] and [K] are temperature dependent heat capacity and thermal conductivity matrices,{T} is the nodal temperature vector, $\left\{\dot{T}\right\}$is the nodal cooling rate vector, and {Q} is the heat flux vector.

The dynamically changing thermal conductivity of the phase mixture is incorporated via ANKOND subroutine. Internal heat generation due to latent heat is simulated by defining a modified specific heat in USPCHT subroutine such that

$$c^* = c + \frac{\dot{\xi}_k}{\dot{T}} L_k \tag{3.2}$$

In heat transfer analysis, it is usually necessary to include nonuniform film coefficients and sink temperatures for the calculation of convection or radiation boundary conditions. The surface temperature dependent convective heat transfer coefficient and sink temperature can be specified using subroutine FILM.

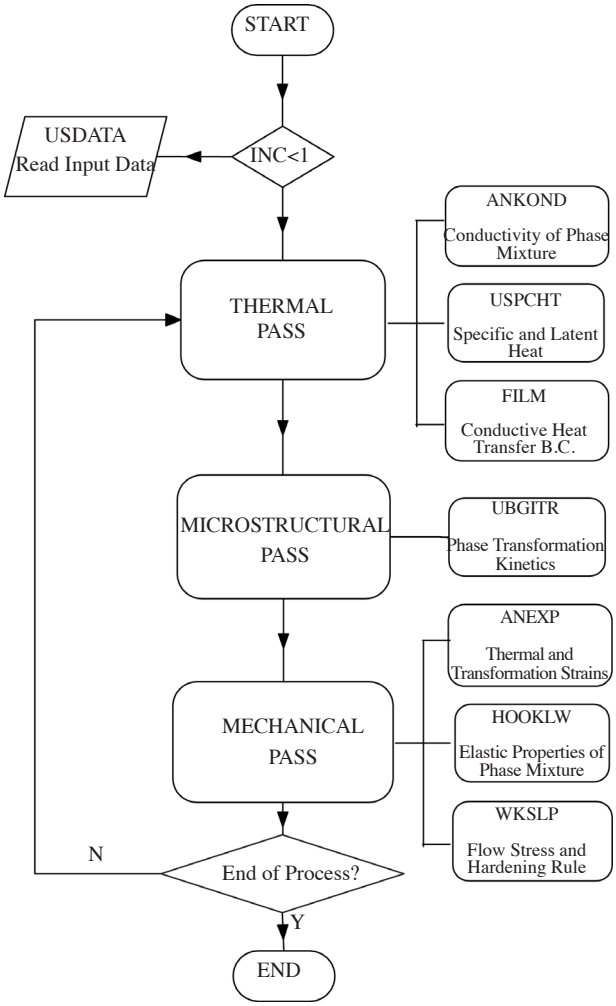

Figure 4. Basic flowchart and subroutines used for implementation of the model.

Microstructural evolution analysis It is convenient to perform phase transformation calculations between the thermal and mechanical analysis. Thus,

the temperature history calculated in the thermal pass can be used in microstructural evolution calculations. Then the microstructural constitution can be used to calculate coupling terms and update material properties for subsequent thermal and mechanical passes. The UBGITR user subroutine is employed for this purpose.

A basic flow chart for UBGITR subroutine is illustrated in Figure 5. First of all, the possibility of a martensitic transformation is controlled in each increment by comparing nodal temperature with martensite start temperature. If martensitic transformation occurs the fraction of martensite is calculated using the Koistinen-Marburger equation. If there is no martensitic transformation, the possibility of a diffusional transformation is checked using the Scheil's sum. If the incubation is complete (S = 1), then transformed amounts are calculated using the JMAK equation and the principle of additivity. Calculated phase fractions are stored in common blocks and written in the post file.

Mechanical Analysis Procedure The mechanical pass is immediately performed after the microstructural analysis. Coupling terms are created using thermal and microstructural analysis results. The governing equations for finite element thermomechanical analysis can be written in the form of

$$[M]\{\ddot{u}\} + [D]\{\dot{u}\} + [K]\{u\} = \{F\} \tag{3.3}$$

$$[H]\left\{\dot{T}\right\} + [C]\{T\} = \{Q\} + \left\{Q^I\right\} + \left\{Q^F\right\} \tag{3.4}$$

where [M],[D], and [K] are the mass, dumping, and stiffness matrices, respectively. $\{Q^I\}$ is the vector of heat generation due to deformation and $\{Q^F\}$ is the heat generated due to friction, which can be safely neglected for the simulation of quenching. All the matrices are temperature dependent except [M].

For the simulation of thermal processing of materials, a commonly used constitutive model for strain increment decomposition is

$$\begin{aligned} d\varepsilon_{ij} &= d\varepsilon_{ij}^{e} + d\varepsilon_{ij}^{p} + d\varepsilon_{ij}^{th} + d\varepsilon_{ij}^{pt} + d\varepsilon_{ij}^{tp} \\ &= d\varepsilon_{ij}^{thermal} + d\varepsilon_{ij}^{\text{mechanical}} \end{aligned} \tag{3.5}$$

in which the total strain increment is divided into thermal and mechanical strain increments. The thermal strain increment consists of thermal and phase transformation strain increments and is defined in user subroutine ANEXP. On the other hand, the mechanical strain increment is composed of elastic and plastic strain increments, which can be calculated using HOOKLW and WKSLP subroutines, respectively.

Application to Steel Quenching

Quench hardening is a common manufacturing process to produce steel components with reliable service properties. A wide spectrum of mechanical properties can be achieved in components via manipulation of the cooling rate. Beside the conventional through-hardening process, most of the surface and thermo-chemical heat treatment processes such as carburizing and nitriding involve a quenching stage. Moreover, thermal surface treatment processes such as induction, flame, or laser hardening also involve a direct quenching stage via a quenchant or indirect quenching via heat conduction through the specimen. Although quench hardening is a vital part of production based on steel, it is also one of the major causes of rejected components, production losses, and components that need to be reworked. Distortion, cracking, achievement of desired distribution of microstructure, and residual stresses are the most important problems during quenching of steels. All these reasons render the prediction and control of the as-quenched state of the component a vital step, in order to reduce production losses and achieve production goals. Based on those facts, the heat treatment industry needs computer simulation of the quenching for the control and optimization of the process parameters.

Experimental procedure

First, C60 steel (0.6% C, 0.25% Si, 0.75% Mn) bars of 30 mm diameter are cut down into cylinders of 60-mm length. Then holes of various diameters are drilled in those specimens. The specimens are labeled as shown in Table 2. Holes in the specimens are closed before heat treatment in order to avoid contact between the quenchant and the inner surface. This will minimize the heat loss from the inner surface and those surfaces are assumed to be insulated for the purpose of the simulation.

During heat treatment, in order to minimize the danger of distortion and cracking, all specimens are preheated at 200 °C for 20 min. Then they are soaked for 30 min at heat treating temperature in a salt bath to prevent decarburization and to ensure uniformity of the temperature and microstructure throughout the entire volume. After the austenization stage, the specimens are immediately quenched

in water at 20 °C. It should be noted that decarburization may drastically alter the residual stress state on the surface (Todinov, 1998). Avoidance of decarburized layer on the surface is essential since the verification of the simulation is based on comparison of surface residual stresses.

X-ray measurements are carried out on a Ψ diffractometer using Cr-Kα radiation on a set of crystallographic planes. Since the peak shift due to lattice strains at high diffraction angles is considerably higher, a peak having high indices and intensity is preferred for measurements. The intensity and angular position data for analysis are provided by scintillation detector and scaler. Counting is undertaken for a fixed time of 2 s at 2θ angles between 152° to 160° by 0.1° steps. The parabola method is used for the determination of the peak maximum and position. Then corresponding values for interplanar spacing and strains are calculated. Finally, the stress is determined by linear regression analysis by determining the slope of the regression line of lattice strain versus $\sin^2\psi$ plot and multiplying it by the elastic modulus of the material. The elastic modulus used in the calculations is the one obtained by mechanical tests. To minimize the instrumental error, adjustment of the measurement system and the effect of specimen curvature on the results are checked by several tests measuring the residual stress on iron powder. To control the reliability and reproducibility of the results, residual stresses are measured repeatedly.

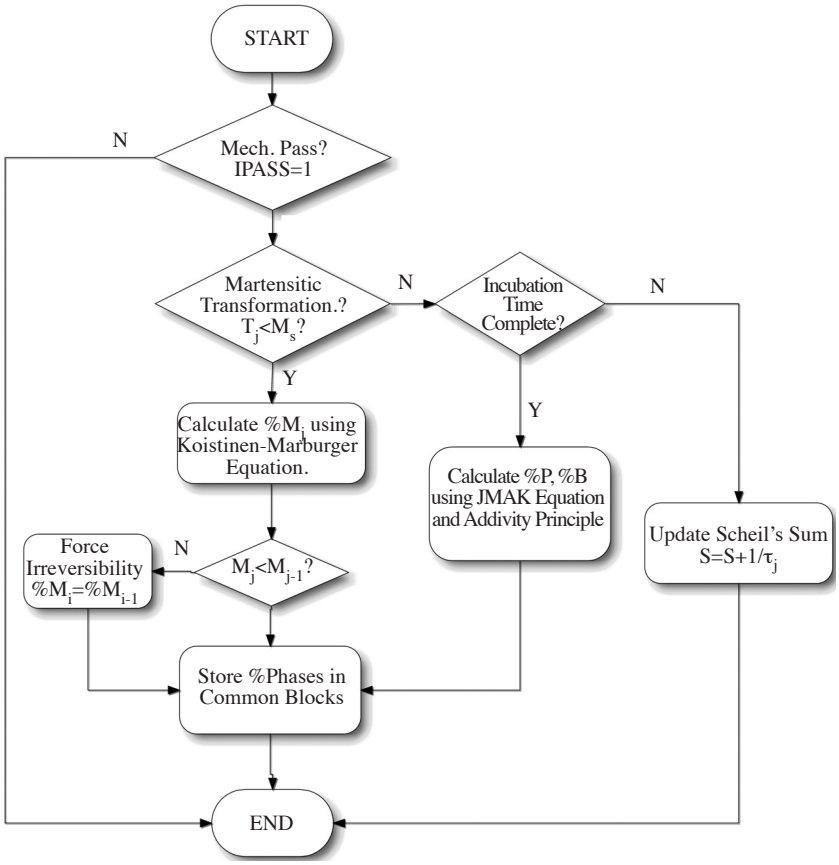

Figure 5. Basic flowchart for microstructural evolution subroutine.

Table 2. Set of specimens used.

Φ = 30 mm , L = 60 mm	S1	S2	S3	S4
Hole Diameter	6 mm	9 mm	12 mm	15 mm

Simulation procedure

Figure 6 illustrates the FE mesh and boundary conditions used in simulations. Using the symmetries, only the required part of the specimen is modeled to improve the efficiency and the stability of the solution. To create the FE mesh 3600 (60 in axial, 60 in radial direction) axisymmetric quadrilateral elements are used. Mesh is refined near the outer surface in order to improve the accuracy of the solution. Due to very large temperature gradients and early phase transformations, those regions are critical for solution accuracy and convergence.

Initially, the temperature is set to 830 °C for all nodes and all of the elements are assumed to consist of 100% homogeneous austenite. A nonlinear convective heat transfer boundary condition is imposed on the outer surface, which is in contact with the quenchant, beside the thermal and mechanical symmetry boundary conditions on the symmetry plane. The surface of the hole is assumed to be insulated. Convective heat transfer coefficient data as a function of surface temperature are presented in Table 3.

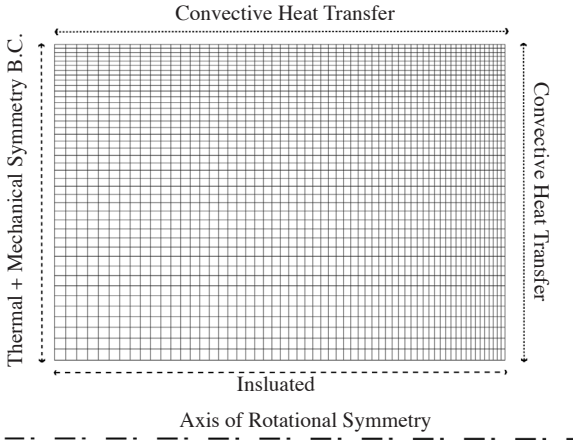

Figure 6. Finite element mesh and boundary conditions used in simulations.

The selection of an appropriate time walk procedure is essential for solution of this highly nonlinear system of equations. A convergence analysis is carried out to ensure convergence at minimum cost. Constant 0.01 s time steps are used in the analysis according to convergence analysis results. The analysis is terminated when all the nodal temperatures are equal to the quenchant temperature (20 °C). Thermo-mechanical data for C60 steel are shown in Table 4.

Table 3. Variation in heat transfer coefficient with temperature (Gur and Tekkaya, 2001).

Temperature (°C)	0	200	400	430	500	560	600	700	800
h (J/m^{2}s°C)	4350	8207	11962	13492	12500	10206	7793	2507	437

Table 4. Thermo-mechanical material data for C60 steel (Gur and Tekkaya, 2001).

Austenite							
T (°C)	E (GPa)	ν	σ_Y (MPa)	H (MPa)	α (μ/°C)	λ (J/ms°C)	C$_\rho$ (MJ/m^3°C)
0	200	0.29	220	1000	21.7	15.0	4.15
300	175	0.31	130	16000		18.0	4.40
600	150	0.33	35	10000		21.7	4.67
900	124	0.35	35	500		25.1	4.90
Ferrite, Pearlite, Bainite							
0	210	0.28	450	1000	15.3	49.0	3.78
300	193	0.30	230	16000		41.7	4.46
600	165	0.31	140	10000		34.3	5.09
900	120	0.33	30	500		27.0	5.74
Martensite							
0	200	0.28	1750	1000	13.0	43.1	3.76
300	185	0.30	1550	16000		36.7	4.45
600	168	0.31	1350	10000		30.1	5
900	124	0.35	35	500		25.1	4.90

Results and discussion

Figure 7 illustrates the comparison of XRD tangential residual stress measurements with the ones predicted by FE simulation. First of all, it can be seen that the predicted surface residual stresses are in good agreement with the experimental ones. Another observation that can be made is that all of the specimens except S1 have tensile type of tangential stresses on the surface. The tangential stress state on the surface is highly dependent on the hole diameter and has an increasing trend with increasing hole diameters. The critical hole diameter, at which the transition from compression to tension occurs, is a function of the hardenability of the steel and the quenching conditions.

Figure 8 illustrates the comparison of the microstructure of the specimen S2 observed in SEM with the one predicted by FE simulation. Predicted axial, radial, and tangential residual stress distribution for the same specimen is also presented in the same figure.

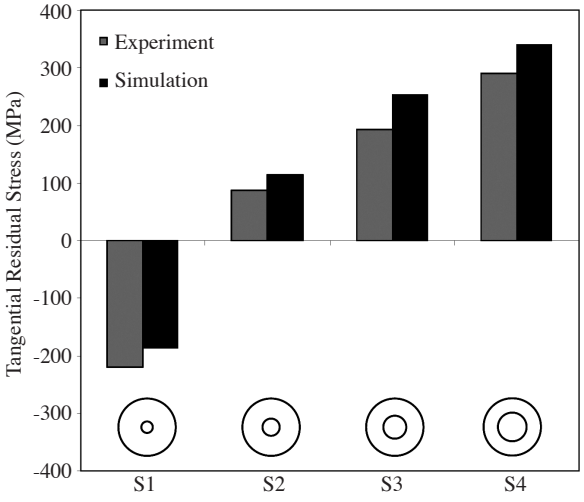

Figure 7. Comparison of tangential residual stress state predicted by computer simulation with XRD diffraction results.

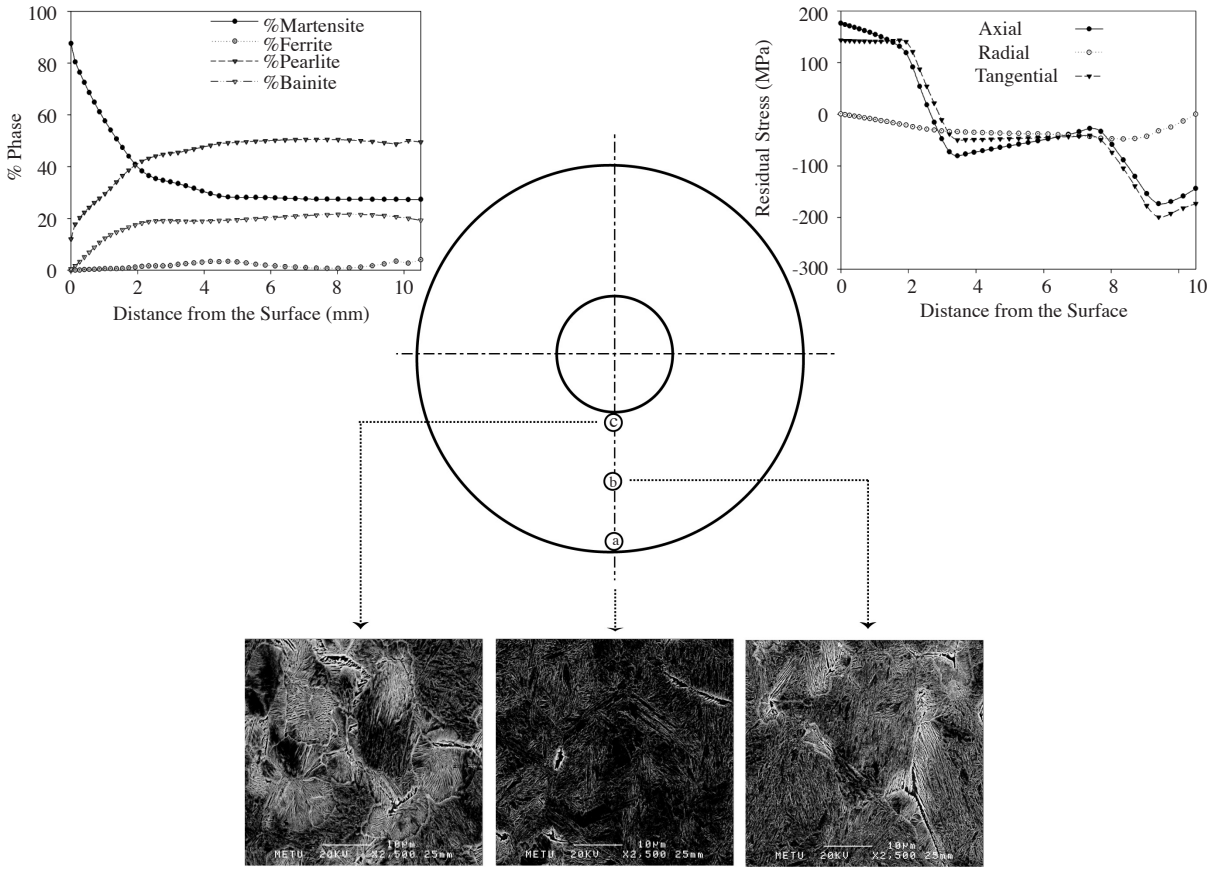

Figure 8. Comparison of SEM micrographs with microstructural evolution predicted by computer simulation.

From the micrograph it can be observed that the outer surface (a) consists of mostly martensite, little bainite/pearlite, and trace amount of ferrite. Simulation results reports 85% martensite, 10% pearlite, and 5% bainite for the same region. Similarly, the mid section (b) is made up of mostly pearlite/martensite mixture, some bainite, and a small amount of ferrite. A composition of 50% pearlite, 33% martensite, 10% bainite, and 2% ferrite is predicted for the same region by computer simulation. Finally, the inner surface (c) has a pearlitic microstructure with some martensite/bainite and an increased amount of ferrite, whereas computer simulation results indicate nearly 55% pearlite, 27% martensite, 14% bainite, and 4% ferrite. All of these results indicate a good match between the calculated and observed microstructures.

Conclusion

Modeling is one of the most crucial elements in the design and optimization of thermal materials processing systems since it provides considerable versatility in obtaining quantitative results, which are needed as inputs for an optimum design cycle. In this study, a mathematical framework capable of predicting temperature history, evolution of phases, and internal stresses during the thermal processing of materials was established. The model was integrated into commercial FEA software Msc.Marc by user subroutines. The accuracy of the model was verified by simulating the quenching of hollow steel cylinders. Simulation results were compared with SEM observations and XRD residual stress measurements. According to the results, it can be concluded that

- The model can effectively predict the trends in the distribution of the microstructure and residual stresses. The accuracy of prediction is also remarkable.
- The model has a modular design that allows simulation of many thermal material processing techniques with minor revisions.
- Determination of final properties of the product after thermal material processing is an involving and challenging task. For example, even the effect of minor geometrical modifications results in large variations in the microstructure and residual stress distribution, which cannot be expressed by a simple rule of thumb.

Nomenclature

Indices

eq	equilibrium value
max	maximum value
o	represents an initial value
k	property related to kth microstructural constituent, any property without subscript k stands for the overall property of the phase mixture.

Operators

$\cdot$	scalar product
$\dot{}$	time derivative
$\ddot{}$	second time derivative
Δ	increment operator
∇	gradient operator
div	divergence operator

Vectors and Tensors

α_{ij}	kinematic hardening (backstress) tensor
δ_{ij}	Kronecker's delta
ε_{ij}	total strain tensor
$\dot{\varepsilon}_{ij}$	total strain rate tensor
$\dot{\varepsilon}^{e}_{ij}$	elastic strain rate tensor
$\dot{\varepsilon}^{p}_{ij}$	plastic strain rate tensor
$\dot{\varepsilon}^{th}_{ij}$	thermal strain rate tensor
$\dot{\varepsilon}^{pt}_{ij}$	phase transformation dilatational strain rate tensor
$\dot{\varepsilon}^{tp}_{ij}$	transformation plasticity (TRIP) rate tensor
σ_{ij}	Cauchy stress tensor
S_{ij}	stress deviator

Matrices and Vectors

[B]	matrix of spatial derivatives of shape functions
[C]	conductivity matrix
[D]	damping matrix
[H]	heat capacity matrix
[K]	stiffness matrix
[M]	mass matrix
{F}	force vector

$\{Q\}$	nodal heat flux vector
$\{Q^I\}$	nodal heat flux vector due to deformation
$\{Q^F\}$	nodal heat flux vector due to friction
$\{T\}$	nodal temperature vector
$\left\{\dot{T}\right\}$	nodal cooling rate vector
$\{u\}$	nodal displacement vector
$\{\dot{u}\}$	nodal velocity vector
$\{\ddot{u}\}$	nodal acceleration vector

Latin Letters

b	time coefficient for JMAK equation
c	specific heat capacity
c^*	fictitious (modified) specific heat
$d\lambda$	plastic multiplier
h	convective heat transfer coefficient
k_B	Stephan-Boltzmann constant
n	time exponent for JMAK equation
r	saturation parameter
t	time
C	kinematic hardening modulus
E	elastic modulus
H	plastic hardening modulus
J_2	second invariant of stress deviator
K	TRIP constant
L	latent heat of transformation
M_s	martensite start temperature
N	number of microstructural constituents
Q^{tr}	internal heat source/sink term
S	Scheil's sum
T	temperature
T_s	surface temperature
T_∞	ambient temperature

Greek Letters

α	linear thermal expansion coefficient
$\bar{\varepsilon}^p$	equivalent plastic strain
κ	hardening parameter
λ	thermal conductivity
ν	Poisson's ratio
ρ	density
σ_o	yield strength
σ_f	flow stress
σ_m	mean stress
τ	fictitious isothermal time
τ_s	transformation start time
ζ	emissivity
ξ	fraction of a microstructural constituent
Δ	structural dilatation due to phase transformation
Φ	heat flux
Ω	Koistinen-Marburger constant
Ψ	yield functional

References

Avrami, M., "Kinetics of Phase Change. I. General Theory", J. Chem. Phys., 7, 1103-1112, 1939.

Cahn, J.W., "Transformation Kinetics During Continuous Cooling", Acta Metallurgica, 4, 572-575, 1956.

Cherkaoui, M., "Transformation Induced Plasticity: Mechanisms and Modeling", Journal of Engineering Materials and Technology-Transactions of the ASME, 124, 55-61, 2002.

Christian, J.W., The Theory of Transformations in Metals and Alloys, Pergamon Press, Oxford, 1975.

Colonna, F., Massoni, E., Denis, S., Chenot, J.L., Wendenbaum, J. and Gauthier, E., "On Thermo-Elastic-Viscoplastic Analysis of Cooling Processes Including Phases Changes", Journal of Materials Processing Technology, 34, 525-532, 1992.

Denis, S., Boufoussi, M., Chevrier, J.C. and Simon, A., "Analysis of the Development of Residual Stresses for Surface Hardening of Steels by Numerical Simulation: Effect of Process Parameters.", International Conference on Residual Stresses (ICRS4), 513-519, 1994.

Denis, S., Farias, D. and Simon, A., "Mathematical-Model Coupling Phase-Transformations and Temperature Evolutions in Steels", ISIJ International, 32, 316-325, 1992.

Denis, S., Gautier, E., Sjostrom, S. and Simon, A., "Influence of Stresses on the Kinetics of Pearlitic Transformation during Continuous Cooling", Acta Metallurgica, 35, 1621-1632, 1987.

Embury, J.D., Deschamps, A. and Brechet, Y., "The Interaction of Plasticity and Diffusion Controlled Precipitation Reactions", Scripta Materialia, 49, 927-932, 2003.

Greenwood, G.W. and Johnson, R.H., "The Deformation of Metals under Small Stresses during Phase Transformations", Proc. Roy. Soc., 283, 403-422, 1965.

Gur, C.H. and Tekkaya, A.E., "Numerical Investigation of Non-Homogeneous Plastic Deformation in Quenching Process", Materials Science and Engineering A, 319, 164-169, 2001.

Hsu, T.Y., "Additivity Hypothesis and Effects of Stress on Phase Transformations in Steel", Current Opinion in Solid State & Materials Science, 9, 256-268, 2005.

Inoue, T. and Wang, Z.G., "Finite Element Analysis of Coupled Thermoinelastic Problem with Phase Transformation", Int. Conf. Num. Meth. in Industrial Forming Processes, 1982.

Inoue, T. and Wang, Z.G., "Coupling between Stress, Temperature, and Metallic Structures During Processes Involving Phase-Transformations", Materials Science and Technology, 1, 845-850, 1985.

Jaluria, Y., "Thermal Processing of Materials: From Basic Research to Engineering", Journal of Heat Transfer-Transactions of the ASME, 125, 957-979, 2003.

Koistinen, D.P. and Marburger, R.E., "A General Equation Prescribing the Extent of the Austenite-Martensite Transformation in Pure Iron-Carbon Alloys and Plain Carbon Steels", Acta Metallurgica, 7, 59-60, 1959.

Loshkarev, V.E., "Mathematical Modeling of the Hardening Process with Allowance for the Effect of Stresses on Structural Transformations in Steel", Metal Science and Heat Treatment, 28, 3-9, 1986.

Magee, C.L., "Transformation Kinetics, Micro-Plasticity and Ageing of Martensite in Fe-31ni", PhD. Thesis, Carnegie Inst. of Tech., Pittsburgh , USA, 1966.

Patel, J.R. and Cohen, M., "Criterion for the Action of Applied Stress in the Martensitic Transformation", Acta Metallurgica, 1, 531-538, 1953.

Rammerstorfer, F.G., Fischer, D.F., Mitter, W., Bathe, K.J. and Snyder, M.D., "On Thermo-Elastic-Plastic Analysis of Heat-Treatment Processes Including Creep and Phase Changes", Computers and Structures, 13, 771-779, 1981.

Rammerstorfer, F.G., Fischer, F.D., Till, E. ., Mitter, W. and Grundler, O., The Influence of Creep and Transformation Plasticity in the Analysis of Stresses Due to Heat Treatment. Numerical Methods in Heat Transfer, 447-460, 1983.

Scheil, E., "Anlaufzeit Der Austenitumwandlung", Arch. Eisenhüttenwes, 8, 565-567, 1935.

Sjöström, S., "Calculation of Quench Stresses in Steel", PhD Thesis, University of Linköping, Linköping, Sweden, 1982.

Sjöstrom, S., "Interactions and Constitutive Models for Calculating Quench Stresses in Steel", Materials Science and Technology, 1, 823-829, 1984.

Todinov, M.T., "Mechanism for Formation of the Residual Stresses from Quenching", Modelling and Simulation in Materials Science and Engineering, 6, 273-291, 1998.

Zandona, M., Mey, A., Boufoussi, M., Denis, S. and Simon, A., Calculation of Internal Stresses during Surface Heat Treatment of Steels. Residual Stresses, 1011-1020, 1993.